Supporting Information for

Unraveling the Origin of the Improved Photovoltaic Performance in Acceptor-Acceptor-Type Perylene-Diimide-Based Polymeric Acceptors through Partially Fluorinating the Benzo[*c*][1,2,5]thiadiazole

Junfeng Tong[a,*], Wuyan Liu[a], Yubo Huang[a], ZheYu Li[a], Yan Wang[b], Suiyan Bai[a], Zezhou Liang[c], Lihe Yan[c,*], Jianfeng Li[a], Yangjun Xia[a,*]

[a]Gansu Provincial Engineering Research Center for Organic Semiconductor Materials and Application Technology, School of Materials Science and Engineering, Lanzhou Jiaotong University, Lanzhou, 730070, China.

[b]Engineering Research Center of Advanced Ferroelectric Functional Materials, College of Chemistry and Chemical Engineering, Baoji University of Arts and Sciences, Key Laboratory of Phytochemistry of Shaanxi Province, Baoji, 721013, PR China.

[c]Key Laboratory for Physical Electronics and Devices of the Ministry of Education & Shaanxi Key Lab of Information Photonic Technique, School of Electronics and Information Engineering, Xi′an Jiaotong University, Xi′an, 710049, China.

E-mail: tongjunfeng139@163.com (J. Tong), E-mail: liheyan@mail.xjtu.edu.cn (L. Yan), xiayangjun2015@126.com (Y. Xia).

1. EXPERIMENTAL SECTION

Table S1 Bandgap, energy level and device parameters of excellent PDI-based conjugated polymers.

Polymer Acceptor	Polymer Donor	E_g^{opt} (eV)	E_{HOMO}/E_{LUMO} (eV)	V_{OC} (V)	J_{SC} (mA cm^{-2})	*FF* (%)	PCE (%)	Ref.
PPDIODT	PBDT-TS1	1.74	–5.90/–3.96	0.76	15.72	55.11	6.58	[1]
RR-P(SePDI)	PTB7-Th	1.74	–5.61/–3.87	0.81	11.80	65.00	6.20	[2]
PDI-V	PTB7-Th	1.74	–5.77/–4.03	0.75	16.20	64.00	7.57	[3]
NDP-V	PTB7-Th	1.91	–5.94/–4.03	0.74	17.07	67.00	8.59	[4]
P1C20	PFDTBT	2.01	–5.59/–3.92	0.88	1.36	25.70	0.31	[5]
PPDI-DTBT	PTB7-Th	1.59	–5.46/–3.87	0.78	10.65	49.00	4.07	[6]
PFPDI-DTBT	PTB7-Th	1.71	–5.75/–4.04	0.76	14.13	58.00	6.23	[6]
PIIG-PDI(OD)	PTB7-Th	1.70	–5.69/–3.99	0.72	8.22	44.20	2.68	[7]
PIP	PTB7-Th	1.56	–5.73/–4.04	0.69	4.15	34.40	0.97	[8]
PQP	PTB7-Th	1.74	–5.97/–3.97	0.71	8.57	57.80	3.52	[8]
PFP	PTB7-Th	1.86	–6.18/–3.95	0.70	5.16	39.30	1.43	[8]
PDPP-PDI	PBDTTT-C-T	1.28	–5.42/–4.07	0.68	7.06	41.78	2.01	[9]

1.1. Syntheses

(1) Bistin DTBTSn and DTFBTSn

Bistins DTBTSn and DTFBTSn were synthesized according to the reported method[10], and molecular structures and purity were characterized by ^{1}H NMR and elemental analyses.

DTBTSn: M.p.,160–165 ℃. ^{1}H NMR (500 MHz, $CDCl_3$), δ (ppm), 8.19 (d, *J* = 3.5 Hz, 2H), 7.88 (s, 2H), 7.30 (d, *J* =3.5 Hz, 1H), 0.43 (t, *J* = 28.0 Hz, 18H). ^{13}C NMR (125 MHz, $CDCl_3$), δ (ppm), 152.7, 145.07, 140.28, 136.12, 128.41, 125.87, 125.84, –8.14. Elemental Anal. Calcd for $C_{20}H_{24}N_2S_3Sn_2$ (%): C, 38.37; H, 3.86; N, 4.47. Found (%), C, 38.22; H, 3.75; N, 4.55.

DTFBTSn: M.p., 150–155 ℃. ^{1}H NMR (500 MHz, $CDCl_3$), δ (ppm), 8.32 (d, *J* = 3.0 Hz, 2H), 8.20 (d, J = 3.0 Hz, 2H), 7.78 (d, *J* = 13.0 Hz, 2H), 7.33 (d, *J* =3.0 Hz, 2H), 7.30 (d, *J* =3.3 Hz, 1H), 0.44 (t, *J* = 28.0 Hz, 18H). ^{13}C NMR (125 MHz, $CDCl_3$), δ (ppm), 157.66, 149.84, 143.61, 141.82, 141.23, 136.17, 135.31, 130.89, 129.24, 125.79, 117.05, 116.80, –8.15. Elemental Anal. Calcd for $C_{20}H_{23}FN_2S_3Sn_2$ (%): C, 37.30; H, 3.60; N, 4.35. Found (%), C, 37.19; H, 3.48; N, 4.42.

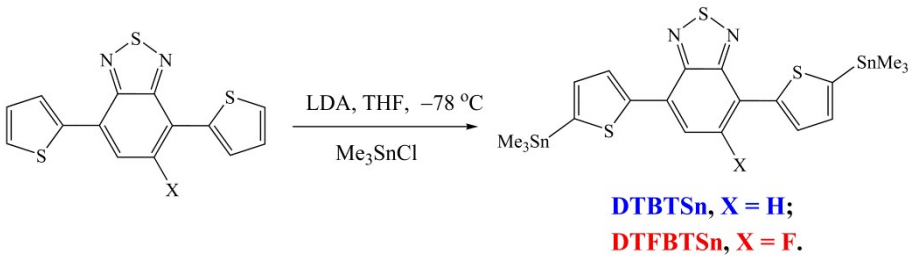

Scheme S1 Synthetic route of bistins DTBTSn and DTFBTSn.

(2) *N*-(2-octyldodecyl)phthalimide (PI-OD)[11]

Under 0 °C, triphenylphosphine (PPh_3, 36.50 g, 139 mmol) and phthalimide (20.50 g, 139 mmol) were added into 500 mL three-neck bottle containing 200 mL CH_2Cl_2. Then 2-octyl-1-dodecanol (28.10 g, 139 mmol) dissolved in 50 mL CH_2Cl_2 (DCM) was added and stirred for 0.5 h before the dropwise addition of diisopropyl azodicarboxylate (28.10 g, 139 mmol diluted with 30 mL DCM) while maintaining the temperature under 10 °C. Upon the complete addition the mixture was stirred for another 1 h at ambient temperature. After re-dissolving in petroleum ether (PE) and filtrating, the crude product was further purified by flash chromatography (silica gel, 200–300 mesh) to obtain the colorless oil. Yield = 52%. ^{1}H NMR (600 MHz, $CDCl_3$), δ (ppm) 7.84 (dd, J = 6.6, 3.6 Hz, 2H), 7.71 (dd, J = 6.6, 3.6 Hz, 2H), 3.57 (d, J =8.4 Hz, 2H), 1.87 (br, 1H), 1.29–1.24 (m, 32H), 0.89–0.85 (m, 6H). Elemental Anal. Calcd for $C_{28}H_{45}NO_2$: C, 78.64%; H, 10.61%; N, 3.28%. Found, C, 78.49%; H, 10.48%; N, 3.35%.

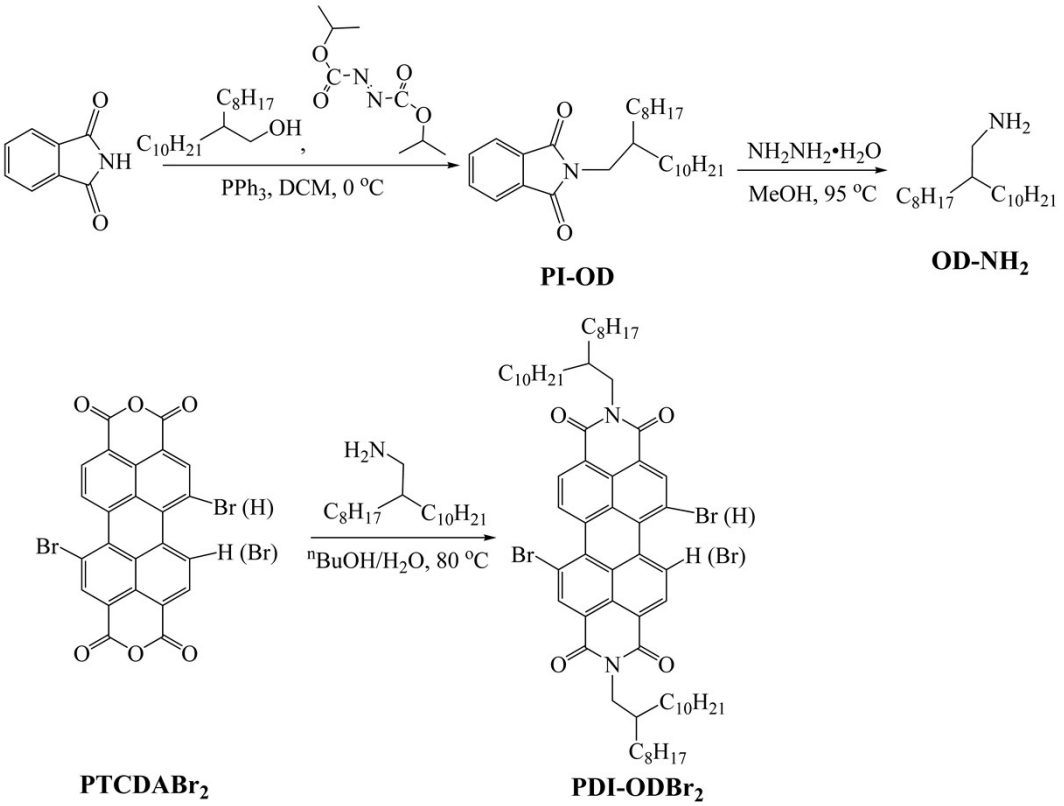

Scheme S2 Synthetic route of dibromide PDI-ODBr$_2$.

(3) 2-Octyldodecyl-1-amine (OD-NH$_2$)[11]

N-(2-octyldodecyl)phthalimide (31.00 g, 73 mmol) was added into 250 mL methanol in the three-neck bottle. Then hydrazine (4.56 g, 73 mmol) was added and the reacting mixture was kept refluxing until the starting material was disappeared. After cooling 2 M KOH was added and the product was extracted with ethyl acetate, washed with brine and dried over Na_2SO_4. The crude oil was purified by chromatography (silica gel, 200–300 mesh) using ethyl acetate (EA) as eluent to

obtain target compound as colourless oil. Yield = 76%. ^{1}H NMR (600 MHz, $CDCl_3$), δ (ppm) 2.59 (d, *J* = 6.0 Hz, 2H), 1.32–1.20 (m, 33H), 1.11 (br, 2H), 0.88 (t, *J* = 7.8 Hz, 6H). Elemental Anal. Calcd for $C_{20}H_{43}N$: C, 80.73%; H, 14.57%; N, 4.71%. Found, C, 80.64%; H, 14.48%; N, 4.82%.

(4) *N*,*N*'-bis(2-octyldodecyl)-(1,7 & 1,6)-dibromo-3,4,9,10-perylene diimide (PDI-ODBr$_2$)[12]

$PTCDABr_2$ (2.00 g, 3.64 mmol) and NH_2-OD (3.80 g, 12.7 mmol) were added into 250 mL three-neck bottle containing 50 mL n-BuOH and 50 mL water. Then sonicated for 10 min and heated at 80 °C to maintain reflux overnight until the starting material was disappeared. After extraction with dichloromethane (DCM) and water, the mixture was purified by chromatography (silica gel, 200-300 mesh) using PE and DCM (PE:DCM=3:1) as eluent to give 1.55 g of the target compound as a dark red solid. Yield = 39%. M.p., 74–76 °C. ^{1}H NMR (600 MHz, $CDCl_3$) δ (ppm) 9.48 (d, *J* = 9.6 Hz, 2H), 8.92 (s, 2H), 8.68 (d, *J* = 9.6 Hz, 2H), 4.17–4.11 (m, 4H), 2.01 (br, 2H), 1.41–1.22 (m, 64H), 0.85 (t, *J* = 7.2 Hz, 12H). ^{13}C NMR (150 MHz, $CDCl_3$) δ 163.20, 162.71, 138.06, 132.91, 132.77, 130.04, 129.22, 128.46, 126.96, 123.80, 123.17, 122.74, 120.80, 44.87, 31.93, 31.91, 30.04, 29.65, 29.36, 29.32, 26.50, 22.69, 14.12. Elemental Anal. Calcd for $C_{64}H_{88}Br_2N_2O_4$: C, 69.30%; H, 8.00%; N, 2.53%. Found, C, 69.19%; H, 7.78%; N, 2.68%.

1.2 Measurement and characterization

^{1}H NMR spectra of the intermediates were characterized on a Bruker XRD-500 Spectrometer in $CDCl_3$ solution as standard (Bruker Instruments, Germany). The thermogravimetric weight is measured by using the TG209F3 thermogravimetric analyser (NETZSCH, USA). Optical contact angle measurement on DSA100 surface tension meter (Kruss, Germany). Cyclic voltammetry (CV) was measured on a CHI electrochemical workstation (Shanghai Chenhua, Shanghai, China) at a scan rate of 100 mV s^{-1} with a nitrogen-saturated solution of 0.1 M tetrabutylammonium hexafluorophosphate (Bu_4NPF_6) in CH_3CN solution. Spin-coating various types of coatings on the devices using a KW-4A desktop leveler (Zhangqiu City Guan Brand Company) and testing the film thickness with a film thickness tester (BRUKER, USA). Vaporized the devices using vacuum coating instrument of model SZZ450 (Shenyang New Blue Sky Vacuum Technology). The devices were irradiated with a solar simulator (San-Ei Electric, Japan) and various important parameters of the PV devices were measured by a solar J-V test system (Keithley, USA). Characterization of the EQE of the device on a 7-SCSpecIII external quantum efficiency measurement instrument (Seven Star Optical Instruments, Beijing, China)。

1.3 Fabrication of PSCs and mobility characterization

Indium tin oxide (ITO) coated glass substrates were washed by a wet-cleaning process inside an ultrasonic bath, with de-ionized water, acetone, de-ionized water and isopropanol in turn. After drying under nitrogen flow, the substrates were treated with oxygen plasma for 10 min, then a thin layer of poly(3,4-ethylenedioxythiophene):poly(styrene-sulfonate) (PEDOT:PSS, ca. 40 nm, Clevios PVP Al4083) was spin-coated onto the ITO substrates and annealed at 150 ºC for 20 min. After that the substrates were transferred into a nitrogen-filled glove box and the active layer was prepared. The active layer, with a thickness in the 100–120 nm range, was deposited on top of the PEDOT:PSS layer by spin-casting from chloroform solution containing the studied materials. The thickness of the active layer was verified by a surface profilometer (DektakXT, Bruker). Then, an ultrathin layer of PDINO (1 mg·mL^{-1} in methanol) was spin-coated on the active layer. Finally, the Al layer (~55 nm) as the cathode was thermally evaporated under a vacuum pressure of 10^{-4} Pa. Moreover, the all effective device area in this work was 0.1 cm^2, which was ascertained by a shadow mask. The thickness values of the evaporated Al was monitored by a quartz crystal thickness/ratio monitor (SI-TM206, Shenyang Sciens Co.). The PCEs of the resulting PSCs were measured under 1 sun, AM 1.5 G (Air mass 1.5 global) condition using a solar simulator (XES-70S1, San-EI Electric Co.) with irradiation of 100 mW·cm^{-2}. The current density-voltage (*J*-*V*) characteristics were recorded with a Keithley 2400 source-measurement unit. The spectral responses of the devices were measured with a commercial external quantum efficiency (EQE)/incident photon to charge carrier efficiency (IPCE) setup (7-SCSpecIII, Beijing 7-star Opt. In. Co.) equipped with a standard Si diode.

The hole-only and electron-only devices were prepared with a diode configuration of ITO/PEDOT:PSS/active layer/MoO_3/Ag or ITO/ZnO/active layer/PDINO/Ag, respectively. The device characteristics were extracted by modeling the dark current under an applied forward bias. The hole and electron mobilities of the active layers were extracted by fitting the current-voltage curves using the Mott-Gurney relationships[S14] (space-charge-limited-current, SCLC). The field dependent SCLC behavior can be expressed as: $J = \frac{9}{8}\varepsilon_0\varepsilon_r\mu\frac{V^2}{L^3}$. Where J stands for the current density, ε_0 is the permittivity of free space (8.85 × 10^{-12} F·m^{-1}), ε_r is the relative permittivity of the transport medium (assumed to be 3, which is a typical value for CPs), μ is the zero-field mobility of hole or electron, L is the thickness of the active layer, and effective voltage $V = (V_{appl} - V_{bi})$, where V_{appl} is the applied voltage to the device and V_{bi} is the built-in voltage. By linearly fitting $J^{1/2}$ with V, the mobilities were extracted from the slope and L: $\mu = \frac{slope^2 \times 8L^3}{9\varepsilon_0\varepsilon_r}$. For the hole-only

devices, V_{bi} is 0 V, while V_{bi} = 0.7 V in the electron-only devices.

1.4. Surface energy calculation[S15,S16]

The surface tension (γ) can be evaluated using the Wu model, *via* Equations (1), (2), and (3), on the basis of the measured contact angles (θ) information.

$$\gamma_{water}(1+cos\Theta_{water}) = \frac{4\gamma_{water}^{d}\gamma^{d}}{\gamma_{water}^{d}+\gamma^{d}} + \frac{4\gamma_{water}^{p}\gamma^{p}}{\gamma_{water}^{p}+\gamma^{p}} \quad (1)$$

$$\gamma_{EG}(1+cos\theta_{EG}) = \frac{4\gamma_{EG}^{d}\gamma^{d}}{\gamma_{EG}^{d}+\gamma^{d}} + \frac{4\gamma_{EG}^{p}\gamma^{p}}{\gamma_{EG}^{p}+\gamma^{P}} \quad (2)$$

$$\gamma = \gamma^{d} + \gamma^{p} \quad (3)$$

Where, γ is the surface energy of the studied semiconductor; γ^{d} and γ^{p} are the dispersion and polar components of γ; γ^{i} is the total surface energy of the i material (i = water or ethylene glycol); γ_i^{d} and γ_i^{p} are the dispersion and polar components of γ_i; and θ is the droplet contact angle (water or ethylene glycol) on the semiconductor film. Flory-Huggins interaction parameter $\chi^{donor-acceptor}$, which is a parameter to evaluate the interaction between polymer donor and polymer acceptor, based on this, the miscibility of the two components can be objectively judged. The smaller the difference of surface energy between donor and acceptor, the lower the value of $\chi^{donor-acceptor}$ and the better the miscibility.

1.6 Femtosecond time-resolved Transient Absorption (fs-TA) Measurements

Fs-TA spectroscopy was performed to measure the temporal evolution of the absorption changes in the excited states, through which the carrier dynamics in femtosecond to nanosecond regime could be revealed. The laser beam is supplied by amplified Ti: sapphire laser source (800 nm, Coherent) that provides 100 fs pulses with a repetition rate of 1 kHz. The output was split into two beams, the stronger one of which was frequency doubled to generate a 400 nm pump light, and the other one was focused into a sapphire plate to generate a broadband supercontinuum probe light. Using an optical chopper, the repetition rate of the pump pulses was adjusted to 500 Hz, and were focused on the sample with the probe pulse (white light). The TA spectra were obtained by comparing the probe light spectra with and without pump light excitation. The photo-induced absorption change as a function of wavelength was described using optical density (absorbance) changes (ΔOD(λ)). By adjusting the delay time between the pump and probe pulses, a 3D transient spectral image ΔOD(λ,t) was formed.

2. Supplementary Figures and Tables

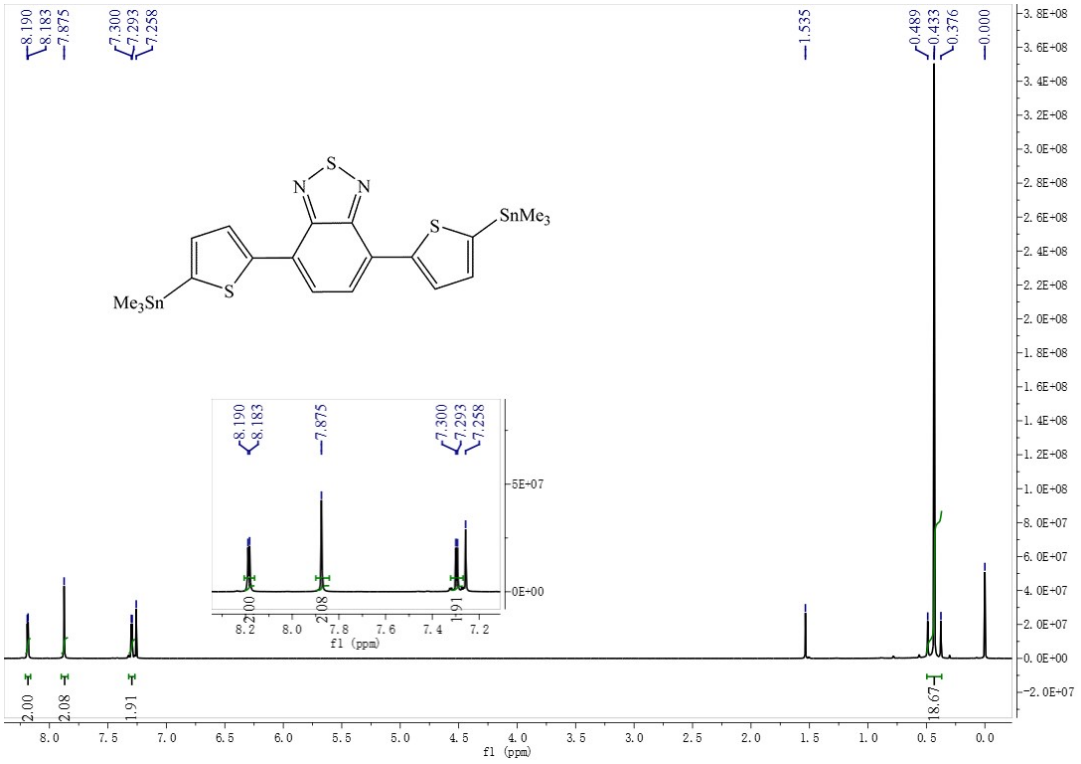

Fig. S1 ^{1}H NMR spectrum of DTBTSn in $CDCl_3$.

Fig. S2 ^{13}C NMR spectrum of DTBTSn in $CDCl_3$.

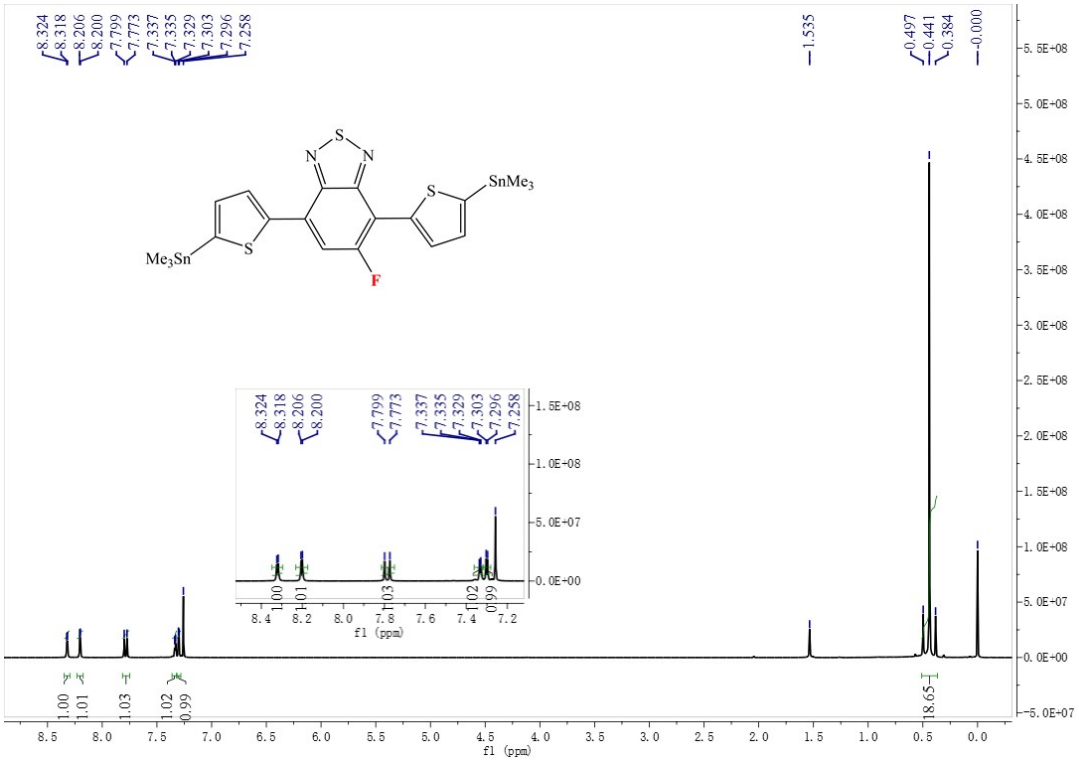

Fig. S3 ^{1}H NMR spectrum of DTFBTSn in $CDCl_3$.

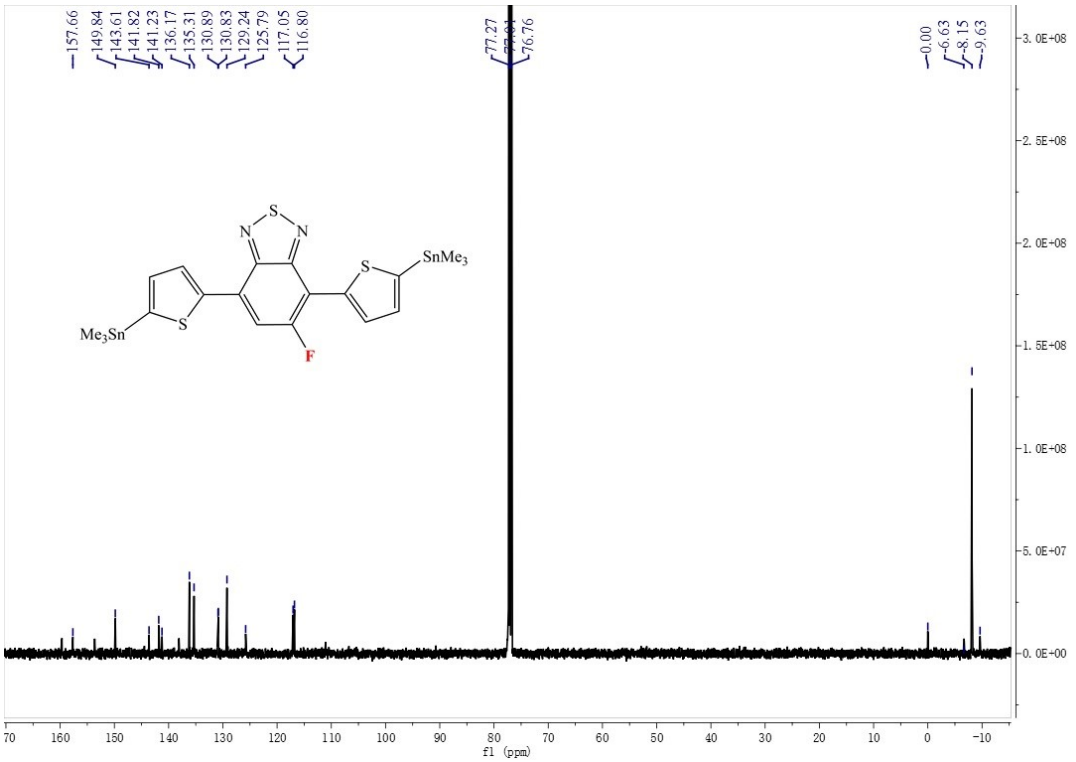

Fig. S4 ^{13}C NMR spectrum of DTFBTSn in $CDCl_3$.

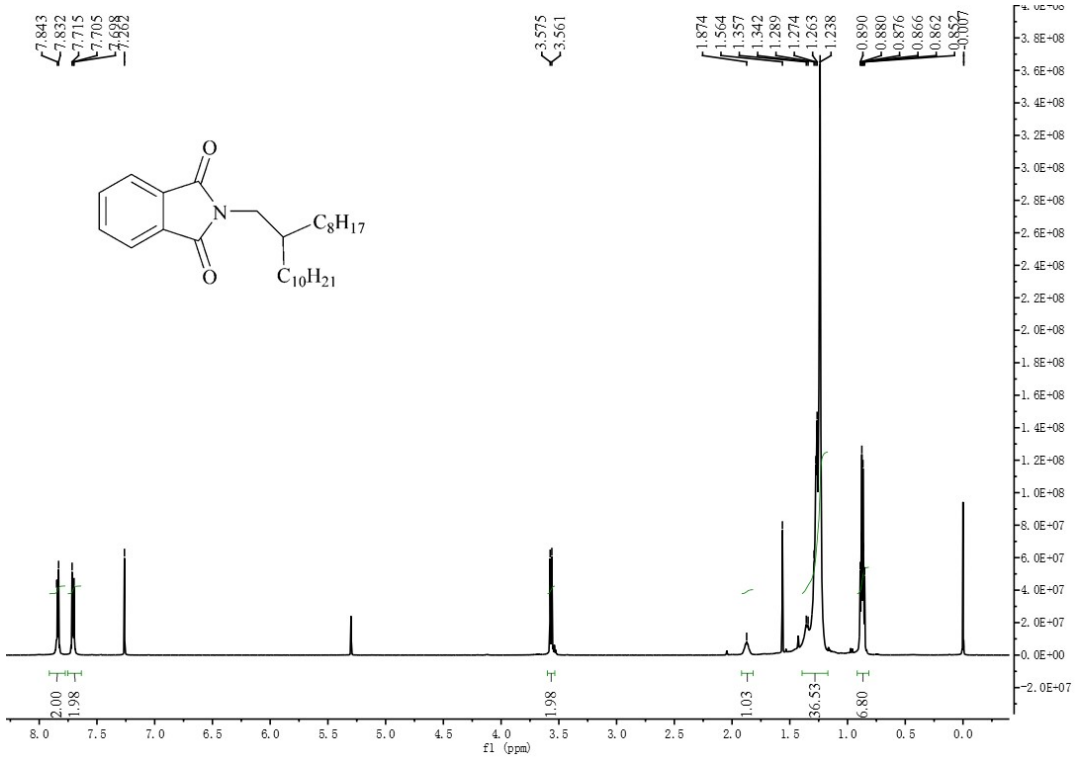

Fig. S5 ^{1}H NMR spectrum of PI-OD in $CDCl_3$.

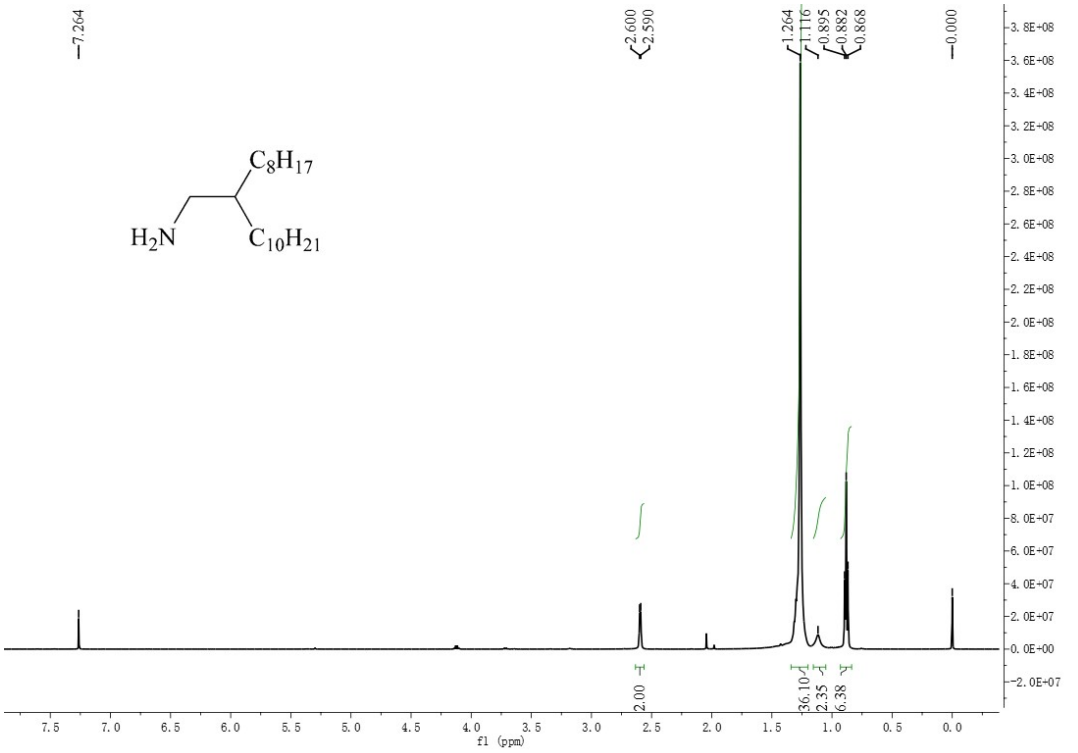

Fig. S6 ^{1}H NMR spectrum of OD-NH_2 in $CDCl_3$.

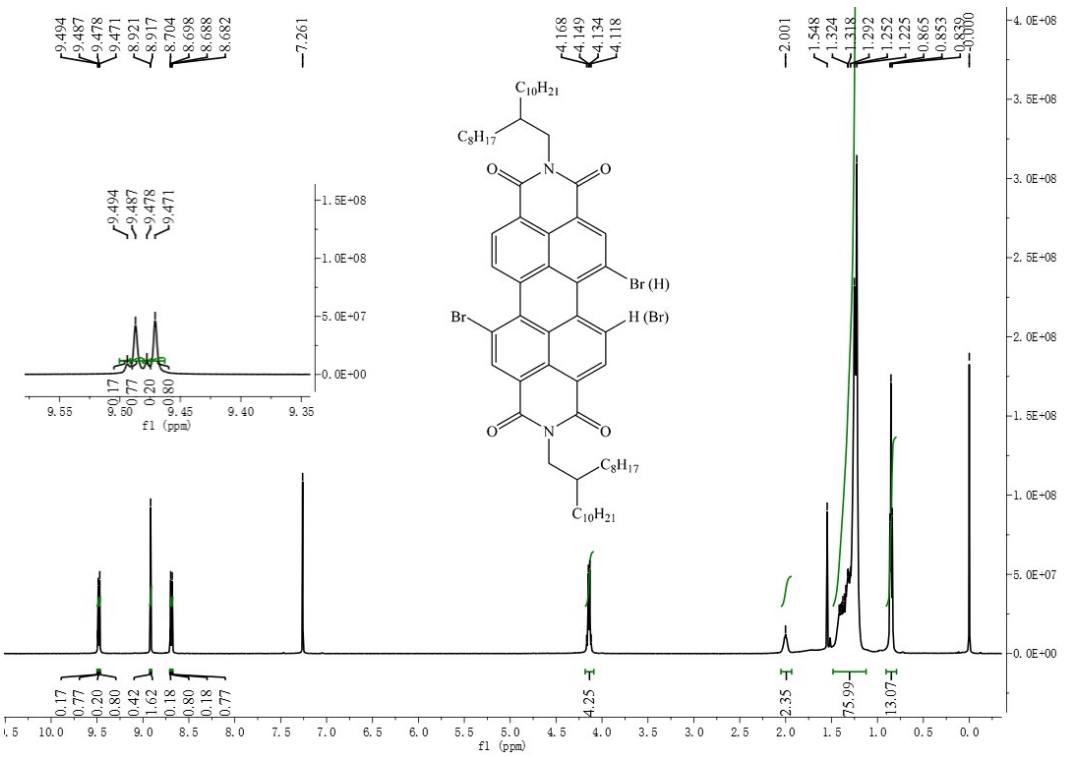

Fig. S7 ^{1}H NMR spectrum of PDI-ODBr$_2$ in CDCl$_3$.

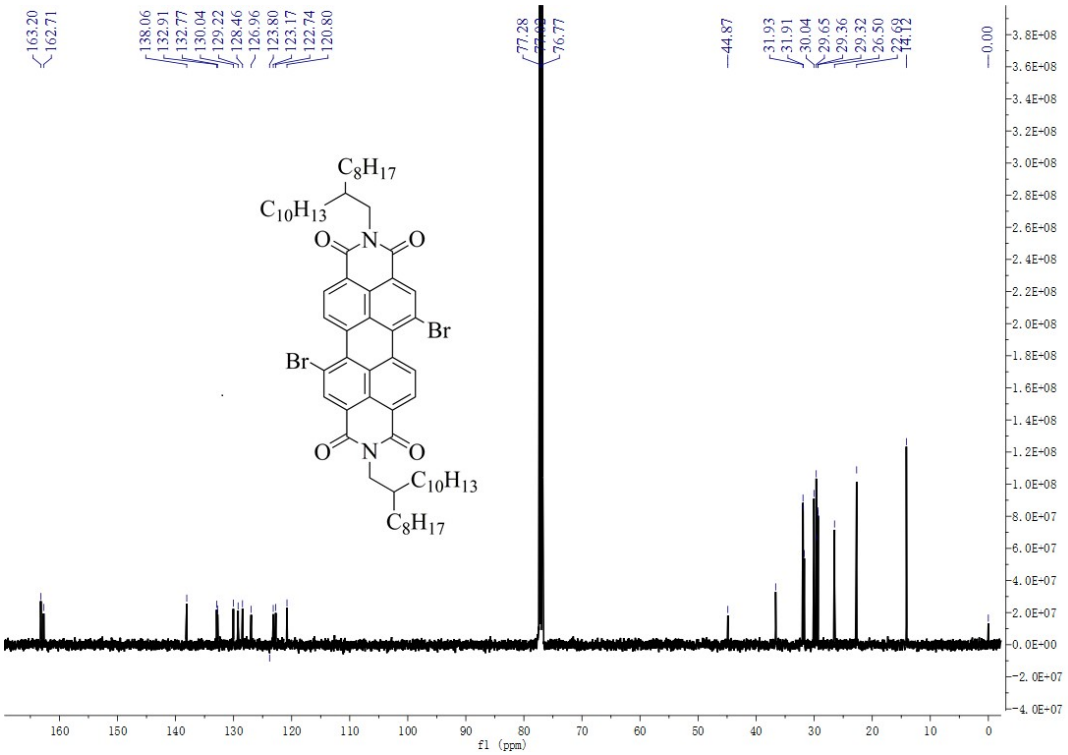

Fig. S8 ^{13}C NMR spectrum of PDI-ODBr$_2$ in CDCl$_3$.

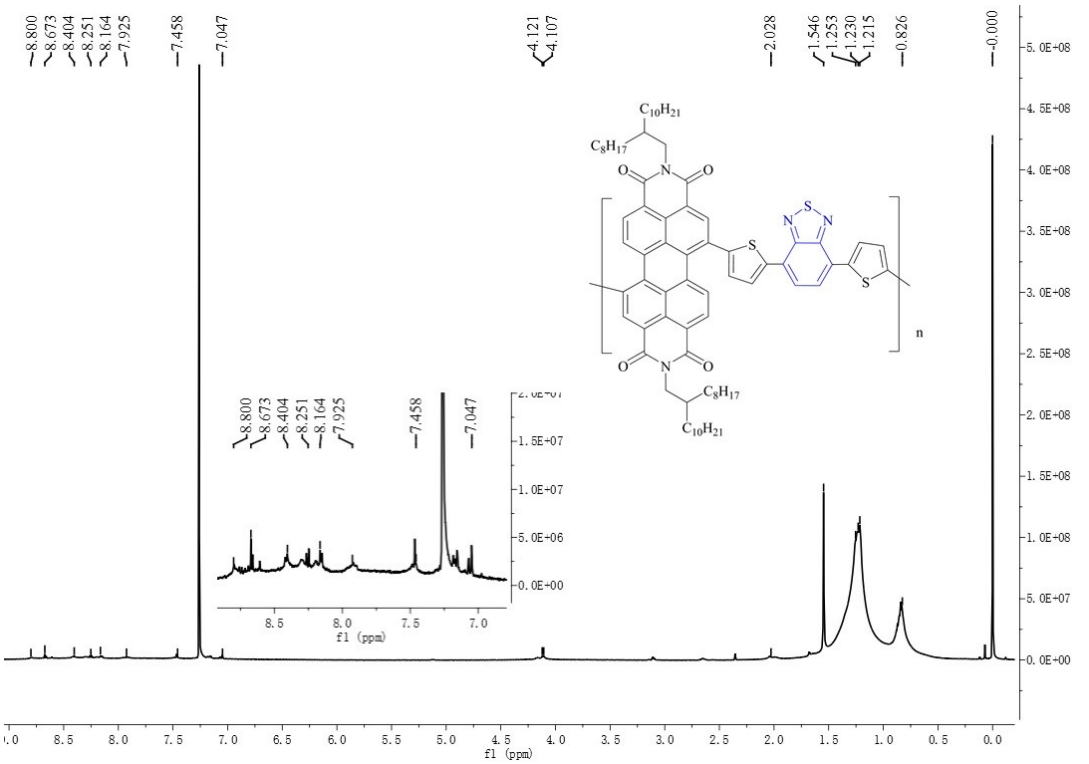

Fig. S9 ^{1}H NMR spectrum of PPDI-DTBT in $CDCl_3$.

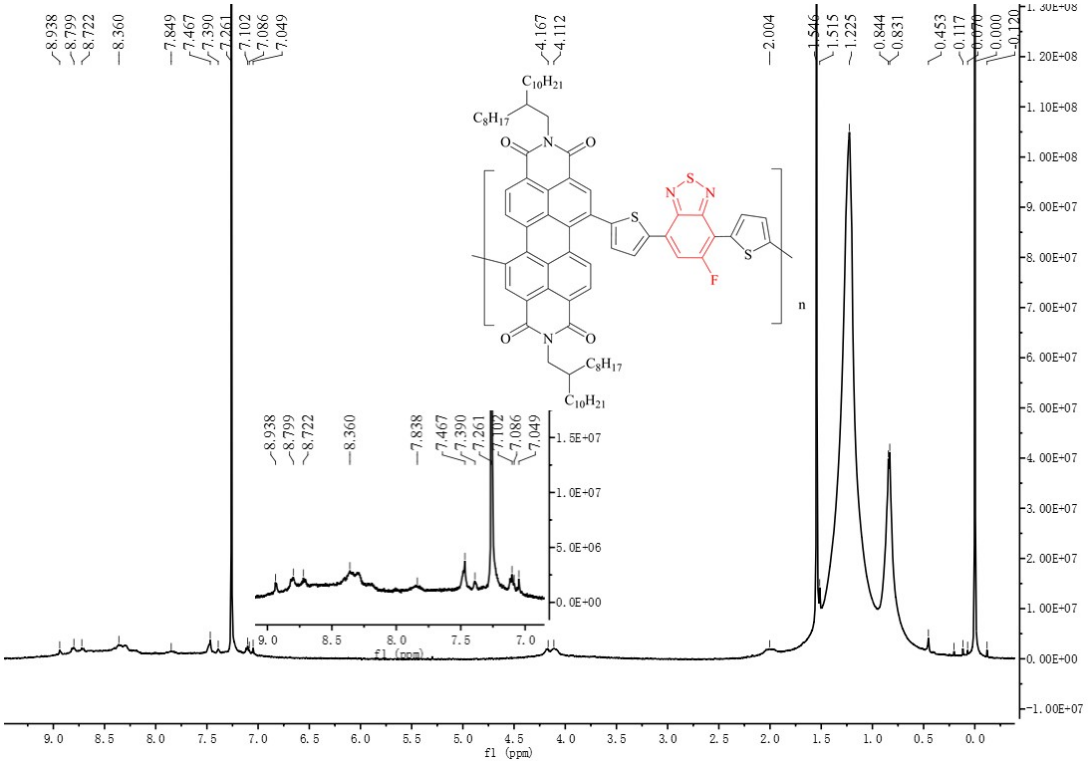

Fig. S10 ^{1}H NMR spectrum of PPDI-DTFBT in $CDCl_3$.

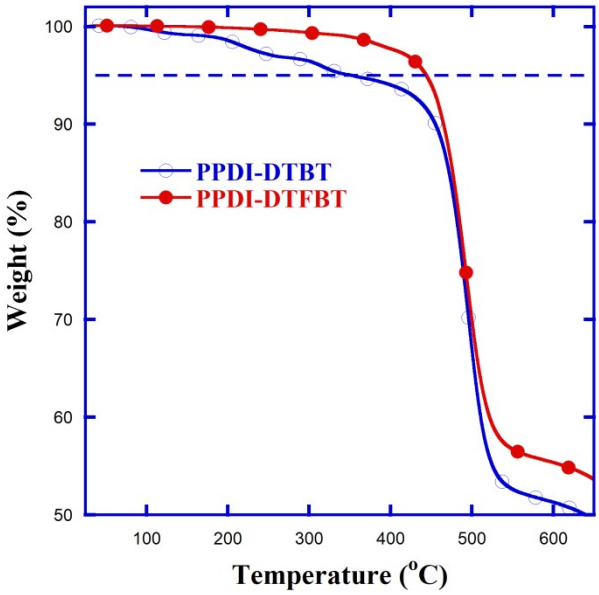

Fig. S11 TG curve of A-A type PDI-based copolymers PPDI-DTBT and PPDI-DTFBT.

Table S2. Yield, GPC, TG data of A-A type polymer acceptors PPDI-DTBT and PPDI-DTFBT.

Polymer	Yield (%)	M_n (kDa)	M_w (kDa)	PDI	T_d (°C)	ε (M^{-1} cm^{-1})	ε (cm^{-1})
PPDI-DTBT	92	13.7	25.3	1.85	352	3.25×10^4 (λ=495 nm)	3.49×10^4 (λ=500 nm)
PPDI-DTFBT	90	12.4	23.7	1.91	444	3.66×10^4 (λ=492 nm)	4.11×10^4 (λ=493 nm)

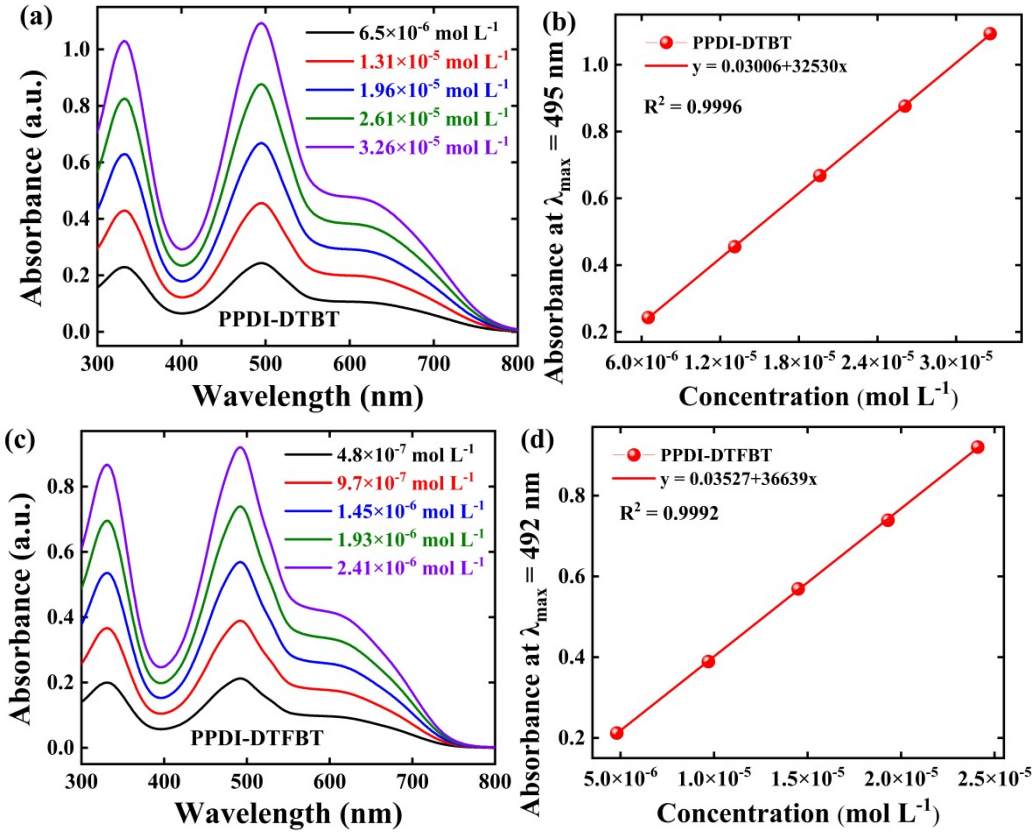

Fig. S12 UV-vis absorption spectra for PPDI-DTBT and PPDI-DTFBT dissolved in solution at varied concentrations (a, c) and the corresponding absorption coefficients (b, d).

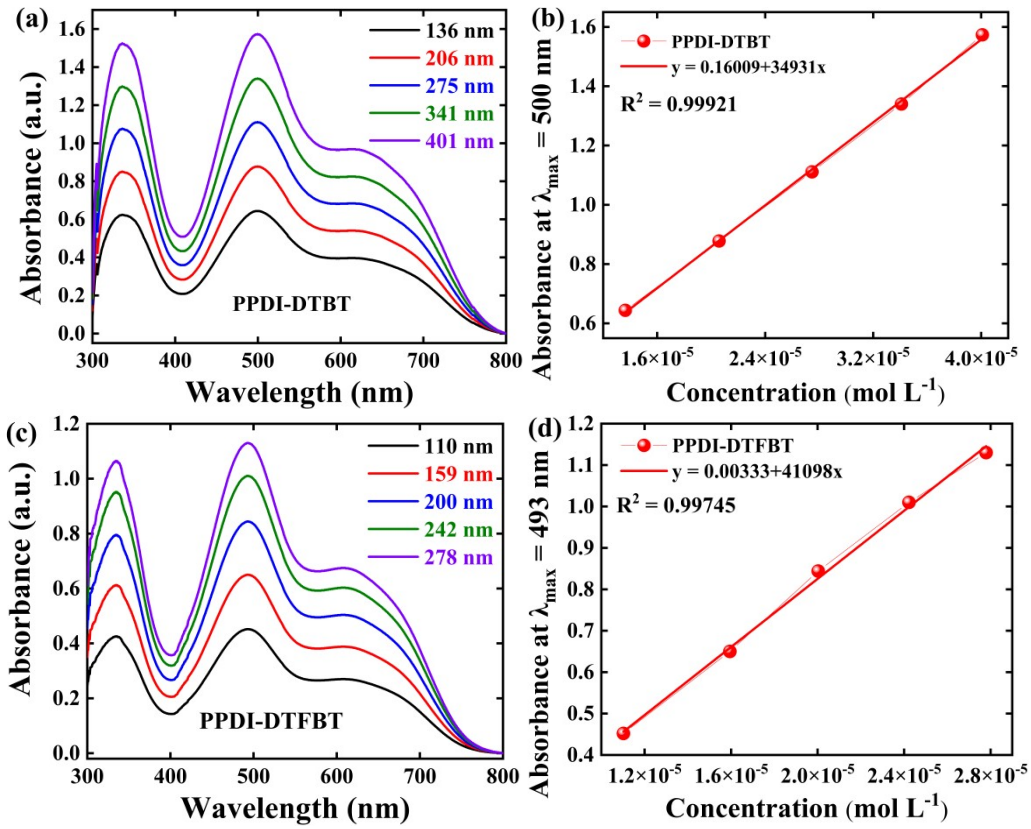

Fig. S13 UV-vis absorption spectra for PPDI-DTBT and PPDI-DTFBT in film state at varied thickness (a, c) and the corresponding absorption coefficients (b, d).

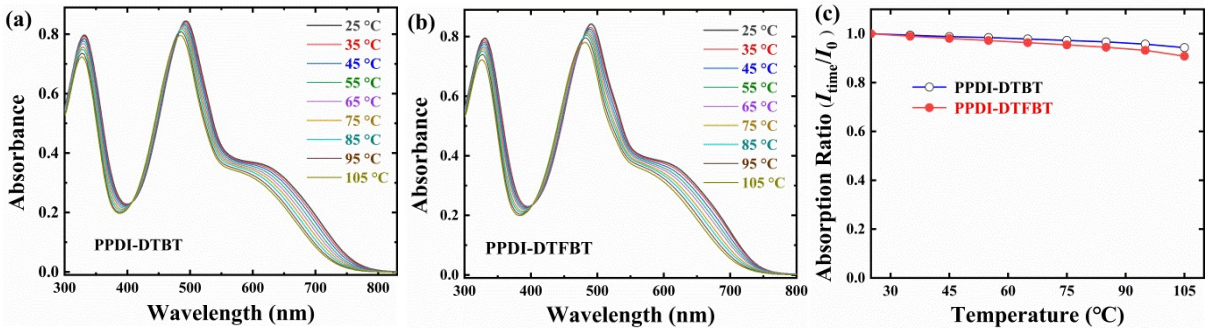

Fig. S14 TD-Abs of PPDI-DTBT (a), PPDI-DTFBT (b) and comparison variation (c).

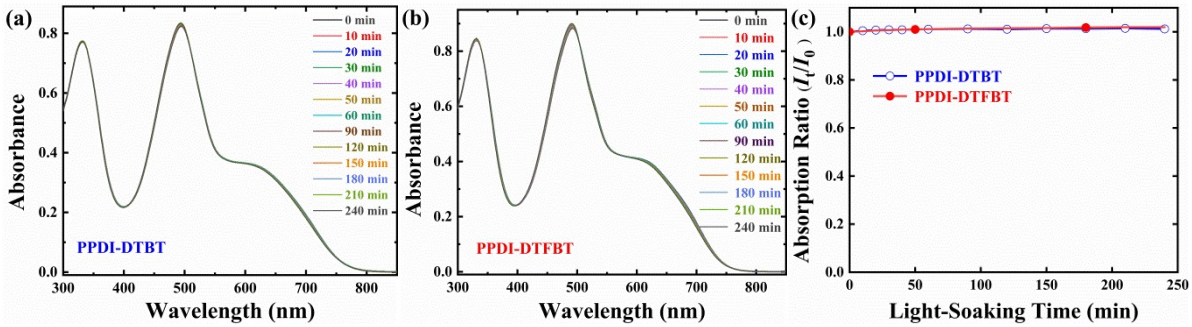

Fig. S15 Absorption variation versus light-soaking time of PPDI-DTBT (a), PPDI-DTFBT (b) and their comparison variation (c)

Table S3 Molecular surface area, MPI extremes of ESP and total average ESP of $(PDI\text{-}DTBT)_2$ and $(PDI\text{-}DTFBT)_2$ and $(TB7\text{-}Th)_2$ simplified from PTB7-Th.

Model Molecules	overall surface area (Å^2)	MPI (kcal/mol)	minimal value (kcal/mol)	maximal value (kcal/mol)	overall average value (kcal/mol)
$(PDI\text{-}DTBT)_2$	1404.51	7.65	–32.99	31.82	1.83
$(PDI\text{-}DTFBT)_2$	1409.09	7.92	–32.71	32.87	1.96
$(TB7\text{-}Th)_2$	1385.25	7.64	–37.97	19.57	–1.61

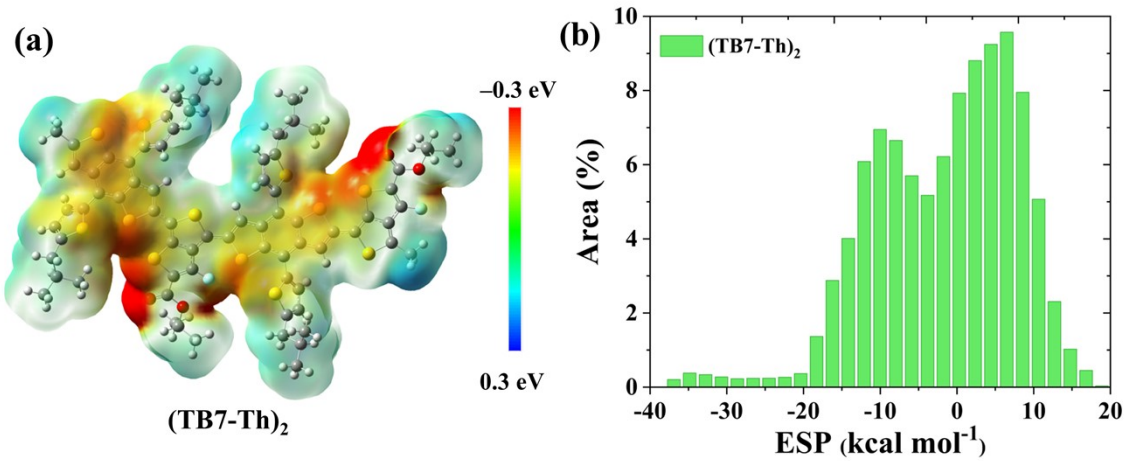

Fig. S16 ESP distribution (a) and ESP area distribution (b) of model compound $(TB7\text{-}Th)_2$ simplified from electron donor PTB7-Th.

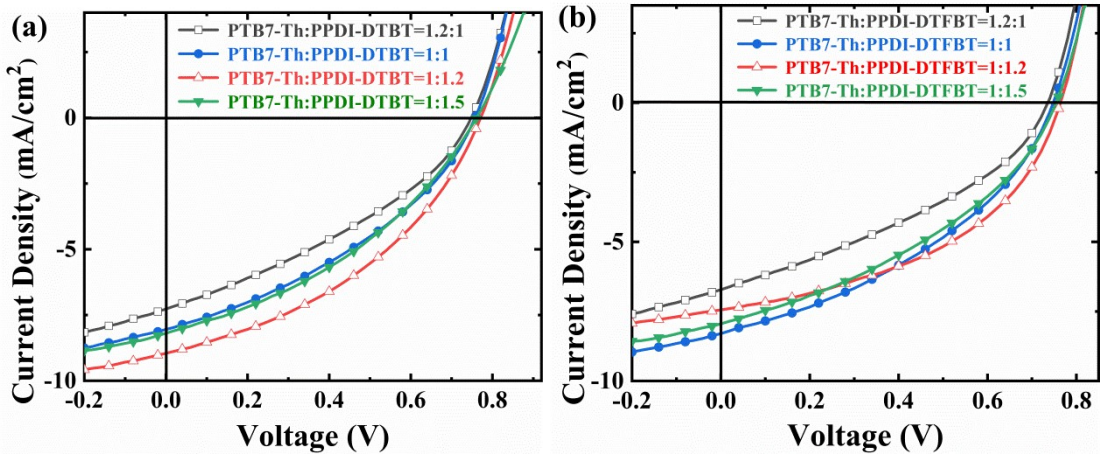

Fig. S17 *J-V* curves of devices based on PPDI-DTBT (a) and PPDI-DTFBT at different weight ratios.

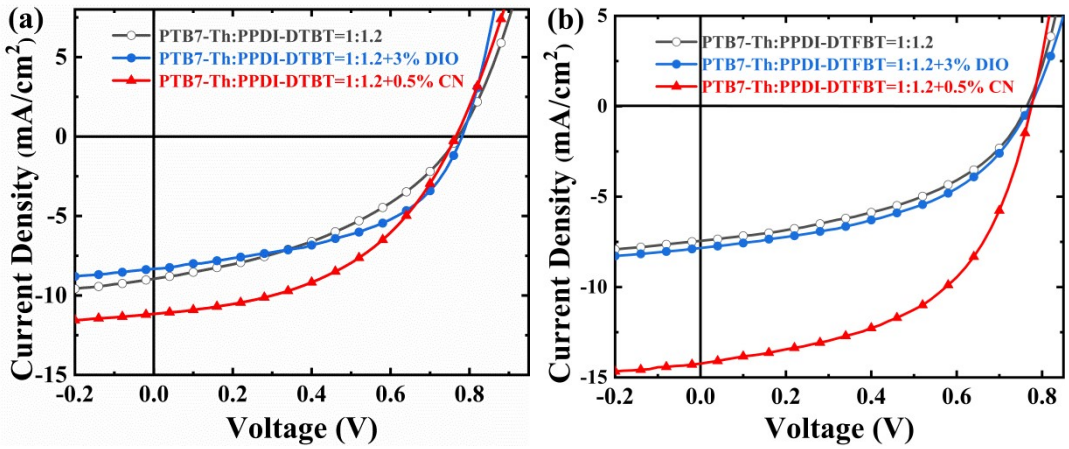

Fig. S18 *J-V* curves of devices based on PPDI-DTBT (a) and PPDI-DTFBT (b) using the solvent additives.

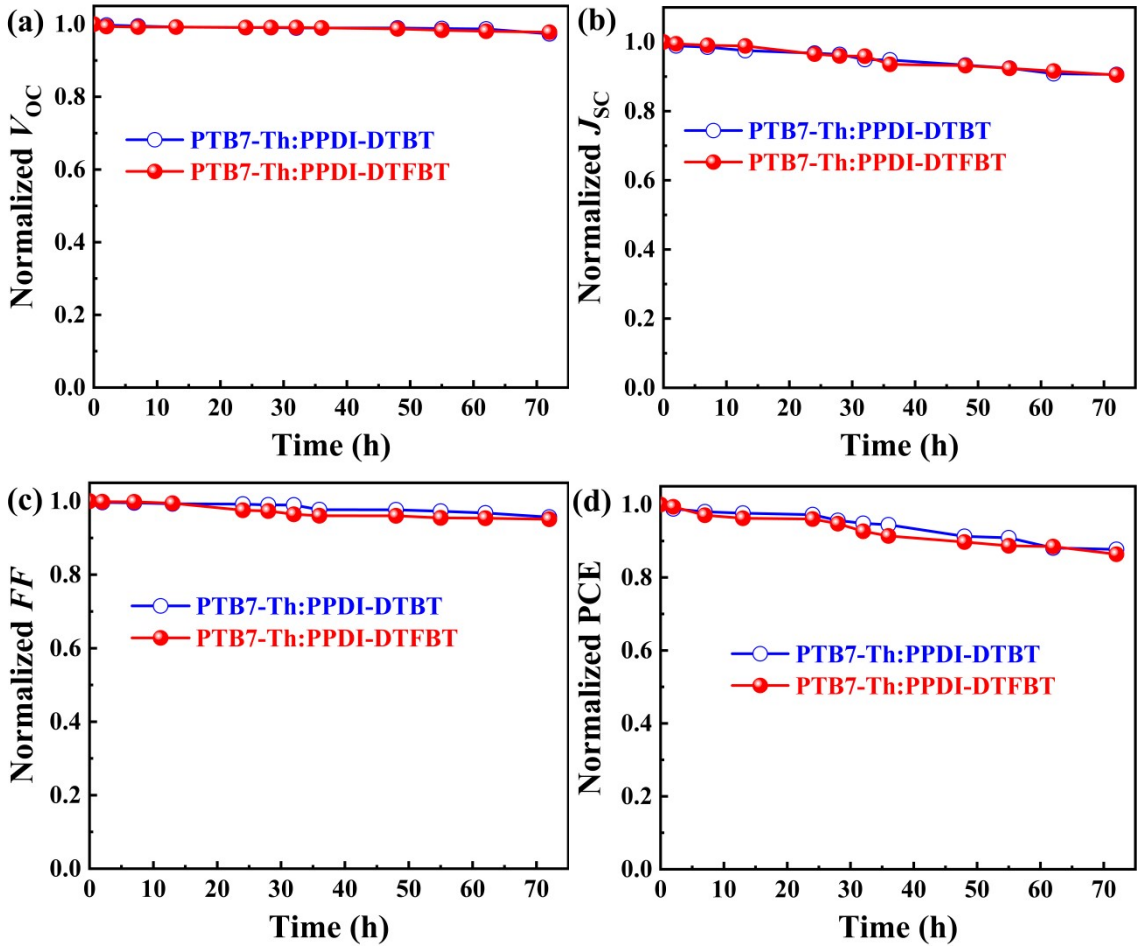

Fig. S19 The storage stability of PTB7-Th:PPDI-DTBT- and PTB7-Th:PPDI-DTFBT-based devices.

Table S4 Device parameters of devices based on PPDI-DTBT and PPDI-DTFBT.

Polymers Acceptor	D:A Ratio /Additive	V_{OC} (V)	J_{SC} (mA cm^{-2})	*FF* (%)	PCE (%)
PPDI-DTBT	1:1.5	0.76	8.19	37.48	2.34
	1:1.2	0.77	8.95	40.10	2.77
	1:1	0.76	8.05	37.18	2.27
	1.2:1	0.75	7.27	34.80	1.89
	1:1.2/3%DIO	0.78	8.32	48.62	3.16
	1:1.2/0.5%CN	0.76	11.10	46.54	3.98
PPDI-DTFBT	1:1.5	0.75	7.94	37.94	2.27
	1:1.2	0.76	7.44	45.50	2.59
	1:1	0.75	8.29	39.08	2.42
	1.2:1	0.74	6.72	35.89	1.77
	1:1.2/3%DIO	0.77	7.84	46.95	2.84
	1:1.2/0.5%CN	0.77	14.73	53.02	6.04

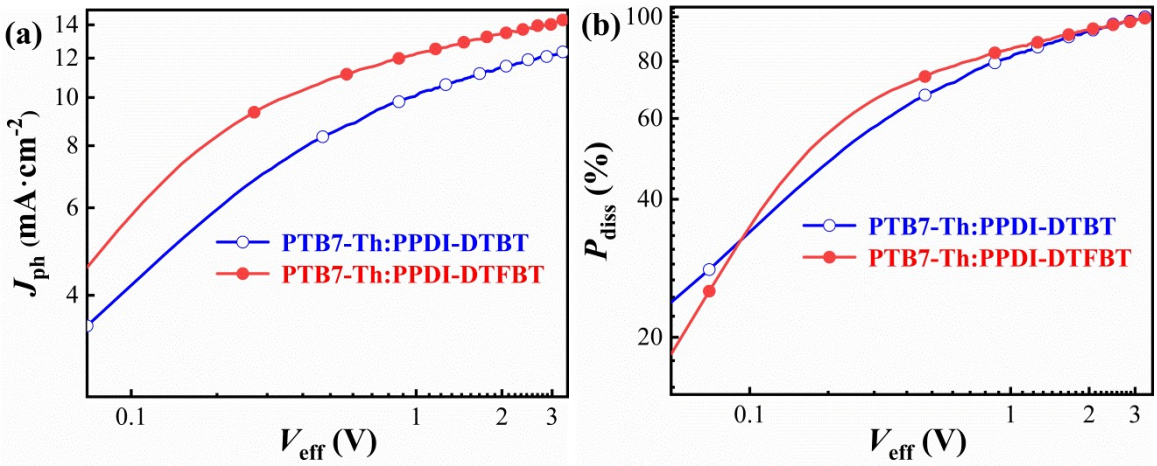

Fig. S20 (a) J_{ph} versus V_{eff} and (b) P_{diss} versus V_{eff} curves for PPDI-DTBT- and PPDI-DTFBT-based devices.

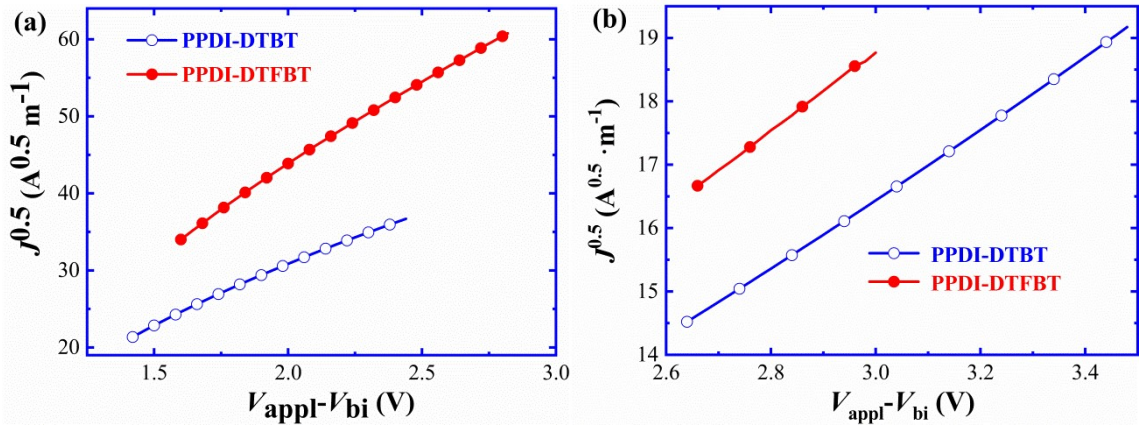

Fig. S21 $J^{0.5}$-V curves of hole-only (a) and electron-only (b) devices under the best fabrication condition.

Table S5 P_{diss}, hole- and electron-mobilities of the optimized devices.

Acceptor	P_{diss}	k_h	Thickness (nm)	μ_h (cm^2 V^{-1} s^{-1})	k_e	Thickness (nm)	μ_e (cm^2 V^{-1} s^{-1})
PPDI-DTBT	77.31%	14.92	110	(9.92±0.2)×10^{-5}	5.53	95	(8.78±0.1)×10^{-6}
PPDI-DTFBT	81.99%	21.73	95	(1.36±0.3)×10^{-4}	6.38	105	(1.58±0.2)×10^{-5}

Table S6 Experimental data obtained from the GIWAXS characterization

Film	Out of plane (010)				In plane (100)			
	Location ($Å^{-1}$)	*d*-spacing (Å)	FWHM	CCL (Å)	Location ($Å^{-1}$)	*d*-spacing (Å)	FWHM	CCL (Å)
PTB7-Th:PPDI-DTBT	1.643	3.82	0.446	12.7	0.260	24.16	0.090	62.8
PTB7-Th:PPDI-DTFBT	1.653	3.80	0.429	13.2	0.262	23.98	0.087	65.0

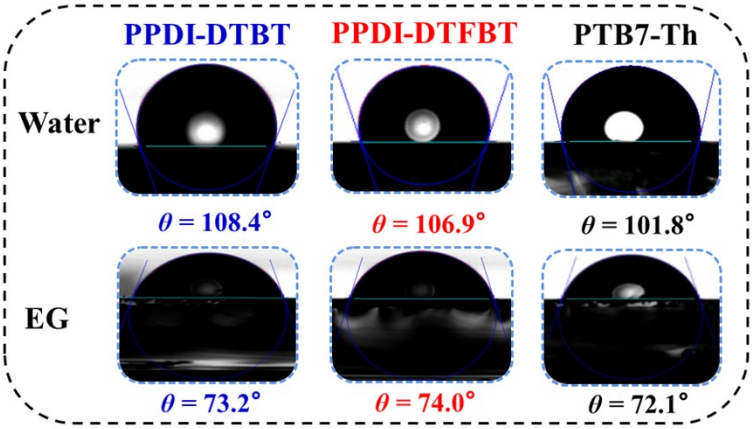

Fig. S22 Contact angle of polymeric acceptors PPDI-DTBT, PPDI-DTFBT and PTB7-Th.

Table S7 Contact angle, surface tension and interaction parameters of PPDI-DTBT, PPDI-DTFBT and PTB7-Th.

Film	Water (°)	EG (°)	γ (mN/m)	$\chi^{donor\text{-}acceptor}$
PTB7-Th	101.8	72.1	29.65	
PPDI-DTBT	108.4	73.2	31.52	0.0286K
PPDI-DTFBT	106.9	74.0	31.81	0.0379K

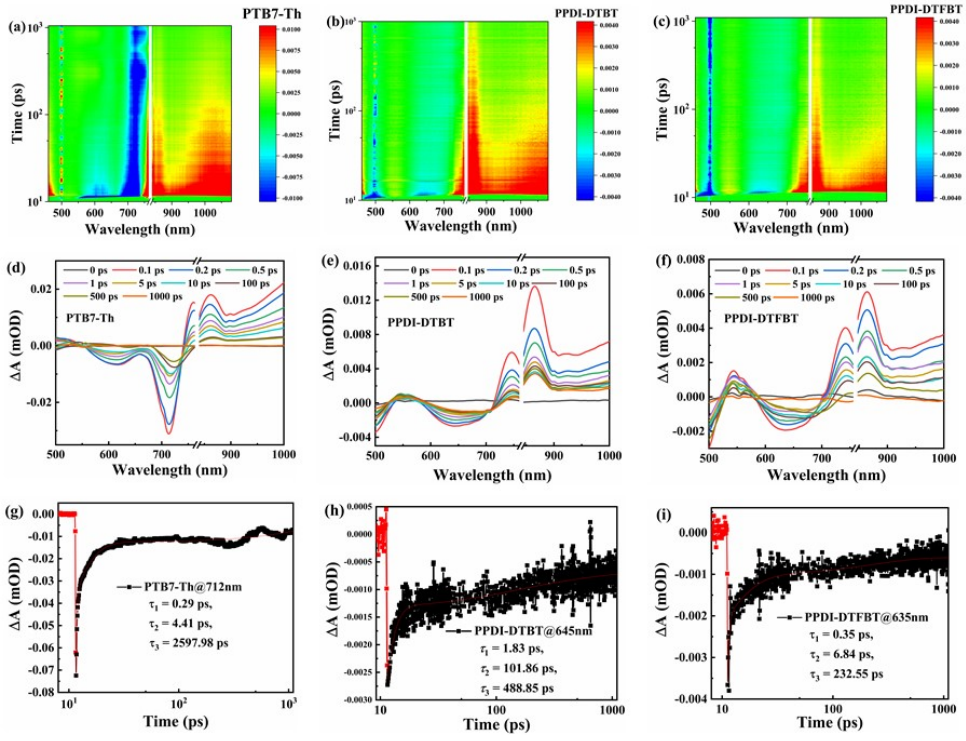

Fig. S23 fs-TA spectra for PTB7-Th (a, d), PPDI-DTBT (b, e) and PPDI-DTFBT (c, f) excited at 400 nm. Kinetics processes for PTB7-Th (g) at 712 nm, PPDI-DTBT (h) at 645 nm and PPDI-DTFBT (i) at 635 nm.

Reference

1 S. Li, H. Zhang, W. Zhao, L. Ye, H. Yao, B. Yang, S. Zhang, J. Hou, *Adv. Energy Mater.*, 2016, **6**, 1501991.

2 Y. Liang, S. Lan, P. Deng, D. Zhou, Z. Guo, H. Chen, H. Zhan, *ACS Appl. Mater. Interfaces*, 2018, **10**, 32397–32403.

3 Y. Guo, Y. Li, O. Awartani, J. Zhao, H. Han, H. Ade, D. Zhao, H. Yan, *Adv. Mater.*, 2016, **28**, 8483–8489.

4 Y. Guo, Y. Li, O. Awartani, H. Han, J. Zhao, H. Ade, H. Yan, D. Zhao, *Adv. Mater.*, 2017, **29**, 1700309.

5 C.-W. Ge, C.-Y. Mei, J. Ling, J.-T. Wang, F.-G. Zhao, L. Liang, H.-J. Li, Y.-S. Xie, W.-S. Li, *J. Polym. Sci. Part A: Polym. Chem.*, 2014, **52**, 1200–1215.

6 M. Liu, J. Yang, Y. Yin, Y. Zhang, E. Zhou, F. Guo, L. Zhao, *J. Mater. Chem. A*, 2018, **6**, 414–422.

7 X. Wang,; L. Lv,; L. Li,; Y. Chen,; K. Zhang,; H. Chen,; H. Dong,; J. Huang,; G. Shen,; Z. Yang,; H. Huang, *Adv. Funct. Mater.*, 2016, **26**, 6306–6315.

8 I. H. Jung, D. Zhao, J. Jang, W. Chen, E. S. Landry, L. Lu, D. V. Talapin, L. Yu, *Chem. Mater.*, 2015, **27**, 5941–5948.

9 Y. Li, Y. Yang, X. Bao, M. Qiu, Z. Liu, N. Wang, G. Zhang, R. Yang, D. Zhang, *J. Mater. Chem. C*, 2016, **4**, 185–192.

10 G. S. Lee, H. J. Shin, S.-B. Lee, H. Choi, Y.-H. Kim, *Macromol. Rapid Commun.*, 2019, **40**, 1800784.

11 J. Tong, X. Jiang, H. Li, L. An, C. Yang, Y. Huang, P. Guo, Z. Liang, C. Yang, J. Li, Y. Xia, *Opt. Mater.*, 2021, **121**, 111593.

12 X. Zhan, Z. Tan, B. Domercq, Z. An, X. Zhang, S. Barlow, Y. Li, D. Zhu, B. Kippelen, S. R. Marder, *J. Am. Chem. Soc.*, 2007, **129**, 7246–7247.